Clim. Past Discuss., 10, 2055–2086, 2014
www.clim-past-discuss.net/10/2055/2014/
doi:10.5194/cpd-10-2055-2014

Climate of the Past Discussions
Open Access

North African vegetation-precipitation feedback in early and mid-Holocene climate simulations with CCSM3-DGVM

R. Rachmayani[1], **M. Prange**[1,2], **and M. Schulz**[1,2]

[1]Faculty of Geosciences, University of Bremen, Klagenfurter Strasse, 28334 Bremen, Germany
[2]MARUM – Center for Marine Environmental Sciences, University of Bremen, Leobener Strasse, 28359 Bremen, Germany

Received: 14 April 2014 – Accepted: 5 May 2014 – Published: 12 May 2014

Correspondence to: R. Rachmayani (rrachmayani@marum.de)

Published by Copernicus Publications on behalf of the European Geosciences Union.

Abstract

The present study analyses the sign, strength and working mechanism of the vegetation-precipitation feedback over North Africa in middle (6 ka BP) and early Holocene (9 ka BP) simulations using the comprehensive coupled climate-vegetation model CCSM3-DGVM. The coupled model simulates enhanced summer rainfall and a northward migration of the West African monsoon trough along with an expansion of the vegetation cover for the early and middle Holocene compared to pre-industrial. It is shown that dynamic vegetation enhances the orbitally triggered summer precipitation anomaly by approximately 20 % in the Sahara/Sahel region (10° N–25° N, 20° W–30° E) in both the early and mid-Holocene experiments compared to their fixed-vegetation counterparts. The primary vegetation-rainfall feedback identified here operates through surface latent heat flux anomalies by canopy evaporation and transpiration and their effect on the mid-tropospheric African Easterly Jet, whereas the effects of vegetation changes on surface albedo and local water recycling play a negligible role. Even though CCSM3-DGVM simulates a positive vegetation-precipitation feedback in the North African region, this feedback is not strong enough to produce multiple equilibrium climate-ecosystem states on a regional scale.

1 Introduction

At present, North Africa is much drier than during the early and middle Holocene when a higher orbitally induced summer insolation triggered more humid and "greener" conditions in the Sahel and Saharan regions (e.g. Kutzbach and Street-Perrot, 1985; Street-Perrott and Perrott, 1993; Jolly et al., 1998; Kohfeld and Harrison, 2000; Prentice et al., 2000; Bartlein et al., 2011; Collins et al., 2013). Following pioneering modelling work by Kutzbach (1981), numerous numerical climate model experiments have been conducted in order to examine climate sensitivity to Holocene orbital forcing in low latitudes, where insolation variations are strongly dominated by the precessional cycle.

CPD
10, 2055–2086, 2014

Even though these model studies have abundantly documented that an intensification and northward shift of the North African summer monsoon was induced by the enhanced seasonal insolation cycle during the early-to-mid Holocene, rainfall anomalies simulated by the models turned out to be significantly smaller than those reconstructed from lake level or pollen data (e.g. Jolly et al., 1998; Kohfeld and Harrison, 2000). Therefore, various positive feedbacks have been postulated to be crucial in shaping the early-to-mid Holocene North African humid period, involving vegetation and soil (e.g. Kutzbach et al., 1996; Claussen et al., 1999; Doherty et al., 2000; Levis et al., 2004a; Hales et al., 2006), sea-surface temperatures (e.g. Kutzbach and Liu, 1997; Zhao et al., 2005; Zhao and Harrison, 2012), and surface-water coverage by lakes and wetlands (e.g. Coe and Bonan, 1997; Krinner et al., 2012). Over time, the notion of a positive vegetation-precipitation feedback has received the greatest attention in the literature (see Claussen, 2009).

Based on early work by Otterman (1974) and Charney (1975), it has been suggested that the effect of an expanded North African vegetation cover on surface albedo would be key in amplifying the early-to-mid Holocene West African monsoonal rainfall (e.g. Claussen and Gayler, 1997; Brovkin et al., 1998; Hales et al., 2006). Provided that the positive vegetation-climate feedback is sufficiently strong to introduce non-linear dynamics into the climate-ecosystem, multiple equilibria of the atmosphere-vegetation state may exist (Claussen, 1994, 1997, 1998; Wang and Eltahir, 2000; Zheng and Neelin, 2000; Renssen et al., 2003; Patricola and Cook, 2008; Bathiany et al., 2012); a humid state with expanded vegetation cover and an arid state with expanded desert. In general circulation and conceptual model studies bi-stability was found only under late Holocene (i.e. after $\sim$6 ka BP) orbital forcing, while only one stable state, the "green (West-) Sahara", was found for early-to-mid Holocene forcing (Claussen and Gayler, 1997; Brovkin et al., 1998; Claussen et al., 1998).

A transition from the humid state to the arid state by a catastrophic bifurcation or "unstable collapse" (Liu et al., 2006, 2007) was suggested to have been abruptly terminating the African humid period around 5.5 ka BP (deMenocal et al., 2000). Both the

CPD
10, 2055–2086, 2014

abruptness of the North African climate transition (Kröpelin et al., 2008; Lézine et al., 2011; Francus et al., 2013) as well as the existence of a strong positive vegetation-rainfall feedback in North Africa (Levis et al., 2004a; Liu et al., 2006, 2007; Kröpelin et al., 2008; Notaro et al., 2008; Wang et al., 2008; Liu et al., 2010) have later been challenged. In a model intercomparison study, two out of three coupled climate-vegetation models that participated in PMIP2 (Paleoclimate Modelling Intercomparison Project, Phase II) suggested a negative vegetation-precipitation feedback over North Africa in simulations of the middle Holocene, though no systematic feedback analysis has been performed (Braconnot et al., 2007). In particular, the Charney feedback operating via surface albedo changes has been called into question (Levis et al., 2004a; Notaro et al., 2008; Patricola and Cook, 2008; Wang et al., 2008; Liu et al., 2010).

In the current study, we investigate the sign, strength and working mechanism of the vegetation-precipitation feedback over North Africa in mid (6 ka BP) and early Holocene (9 ka BP) simulations with the comprehensive fully coupled climate-vegetation model CCSM3-DGVM. In contrast to statistical (lagged autocovariance) approaches (e.g. Notaro et al., 2008; Wang et al., 2008) to assess the existence and sign of the biogeophysical feedback, we apply a straightforward experimental design to assess the climate-vegetation feedback in North Africa by switching on and off interactive dynamic vegetation in this specific coupled model. Moreover, the impact of vegetation initial conditions on mid-Holocene and modern (pre-industrial) climate-vegetation simulations and hence the existence of multiple equilibria in the North African climate-ecosystem is systematically studied.

2 Experimental design

2.1 Model

The National Center for Atmospheric Research (NCAR) Community Climate System Model version 3 (CCSM3) is composed of four components representing atmosphere,

CPD
10, 2055–2086, 2014

ocean, land (including the Dynamic Global Vegetation Model; DGVM) and sea ice connected by a flux coupler (Collins et al., 2006). Here we use the low-resolution version of the model, in which the resolution of the atmosphere and land components is given by T31 (3.75° transform grid), while the ocean has a nominal horizontal resolution of 3° (Yeager et al. , 2006). The atmospheric and oceanic grids have 26 and 25 levels in the vertical, respectively. New parameterizations for canopy interception and soil evaporation have been implemented into the land component in order to improve the simulation of the land hydrology and vegetation cover (Oleson et al., 2008) as in Handiani et al. (2013). CCSM3's dynamic vegetation model DGVM is based on the Lund-Potsdam-Jena (LPJ) model (Sitch et al., 2003; Levis et al., 2004b; Bonan and Levis, 2006) and simulates the tempo-spatial distribution of 10 plant functional types (PFTs; 7 tree PFTs and 3 grass PFTs) which are differentiated by physiological, morphological, phenological, bioclimatic, and fire-response attributes (Levis et al., 2004b). The land and atmosphere components are integrated with a 30 min time step, while vegetation structure and PFT population densities are updated annually (Levis et al., 2004b).

2.2 Setup of experiments

In order to disentangle the impact of dynamic vegetation on the early and mid-Holocene North African climate three sets of experiments were carried out. The first set (OAV) uses the fully coupled CCSM3-DGVM inluding dynamic ocean (O), atmosphere (A), and vegetation (V) components as described above. A pre-industrial (PI) control run of CCSM3-DGVM was performed following the PMIP2 protocol with respect to the forcing (Braconnot et al., 2007). The PI simulation was integrated for 1000 years upon initialization with present-day hydrographic data and bare soil. Branched off from year 600 of the PI run, a middle (6 ka BP) and an early Holocene (9 ka BP) climate simulation was performed, each integrated for 400 years. Table 1 summarizes radiative forcings used in the set of model runs. Since variations in greenhouse gas concentrations over the three time slices are minor, the major forcing comes from variations in the Earth's orbital parameters. The orbitally induced summer insolation anomaly is larger at 9 ka BP than

CPD
10, 2055–2086, 2014

at 6 ka BP (Berger, 1978). The experiments with dynamic vegetation are referred to as 0k(OAV), 6k(OAV), and 9k(OAV), respectively. To examine the role of DGVM initial conditions and the potential for bistable climate-vegetation states, two additional 400-year long CCSM3-DGVM simulations for PI and the mid-Holocene were carried out, which were also initialized from year 600 of 0k(OAV) except for the vegetation cover (PFT distribution), which was taken from the final state of the 9k(OAV) experiment. These simulations are denoted by 0k9k(OAV) and 6k9k(OAV), respectively.

In the second set of experiments (OAV_f) the global PFT distribution is fixed. Three experiments with PI, 6 ka BP, and 9 ka BP boundary conditions (Table 1) were integrated for 400 years (again branched off from year 600 of 0k(OAV)) using the fixed vegetation cover taken from the final state of experiment 0k(OAV). These experiments are denoted by 0k(OAV_f), 6k(OAV_f), and 9k(OAV_f). The third set of experiments (OA) is identical to the OAV_f set of experiments, except that the observation-based modern vegetation cover from the standard CCSM3 setup without DGVM was prescribed. These runs are referred to as experiments 0k(OA), 6k(OA), and 9k(OA).

In all simulations, ozone and aerosol distributions were kept at pre-industrial levels (Otto-Bliesner et al., 2006), and a fixed solar constant of 1365 $W m^{-2}$ was applied. Moreover, all experiments were run with modern ice-sheet configuration and global sea level. For model output analyses, averages of the last 100 simulation years from each experiment were used and are presented here. Since this study focusses on the West African summer monsoon system, the analysis of climatologic quantities is limited to the months of June through September (JJAS). Note that a present-day calendar is used for all experiments.

3 Results

The North African vegetation cover from the 0k(OAV) control run is shown in Fig. 1, where the 10 PFTs simulated by the model are combined into two groups (trees and grasses). North of 18° N the model simulates desert with almost no vegetation.

CPD
10, 2055–2086, 2014

Between 12° N and 18° N, a semi-arid belt dominated by C_4 grass vegetation is simulated. To the south, the simulated vegetation cover mostly consists of trees in central and western tropical Africa. Similar to earlier dynamic vegetation modelling studies (Bonan et al., 2003; Sitch et al., 2003; Oleson et al., 2008), CCSM3-DGVM produces too much forest cover south of the Sahel compared to satellite observations (DeFries et al., 1999, 2000; Lawrence and Chase, 2007). Applying mid-Holocene boundary conditions in experiment 6k(OAV) results in a northward expansion of the North African vegetation cover (Fig. 2a), which is even more pronounced in experiment 9k(OAV) under early Holocene boundary conditions (Fig. 2b). The vegetation increase also captures the Arabian Peninsula and is mostly due to expansion of grasses.

Figure 3a and b support that the greening of North Africa in the early-to-mid Holocene is associated with enhanced summer (JJAS) precipitation over this region, with largest rainfall anomalies between 10° N and 25° N. Averaged over this latitude range and between 20° W–30° E, the mid-Holocene summer rainfall anomaly amounts to 0.97 mm day^{-1} and lies well within the range of previously published 6 ka BP climate model simulations (Braconnot et al., 2007). For the 9k(OAV) simulation, the summer rainfall anomaly over this region is even larger (1.27 mm day^{-1}) due to stronger orbital forcing (Table 1). Southwesterly surface wind anomalies between 15° N and 25° N indicate that the enhanced precipitation is associated with a northward expansion of monsoon winds and a northward displacement of the monsoon trough (Fig. 3a and b).

In the simulations with fixed modern vegetation biogeography (OAV_f) the middle and early Holocene rainfall anomalies over North Africa are significantly smaller compared to their OAV counterparts (Fig. 3c–f). Averaged over the Sahara/Sahel region 10° N–25° N, 20° W–30° E the summer anomalies amount to only 0.80 and 1.04 mm day^{-1} for experiments 6k(OAV_f) and 9k(OAV_f), respectively, relative to PI. This result indicates a positive vegetation-precipitation feedback in North Africa. For both the 6 and 9 ka BP time slices, the implementation of the interactively coupled DGVM into the climate model enhances the orbitally triggered rainfall anomaly over the Sahara/Sahel region by approximately 20 %. Experiments without dynamic vegetation using the standard

CPD
10, 2055–2086, 2014

CCSM3 setup (OA) yield early and mid-Holocene rainfall anomalies over North Africa that are similar to the OAV_f results (Table 2).

The wetter North African conditions in the early and mid-Holocene OAV experiments compared to their OAV_f counterparts are not associated with a wholesale strengthening of the southwesterly monsoon flow that transports moist air from the equatorial Atlantic to the continent (Fig. 3e and f). However, spatially coherent anomalies in the wind system over North Africa can be found at mid-tropospheric levels related to changes in the African Easterly Jet (AEJ), which constitutes the equatorward portion of the Saharan High and dominates the sub-Saharan summer circulation over West Africa between 10° N and 20° N with maximum wind speeds between 700 hPa and 500 hPa. In all early and mid-Holocene simulations, a westerly wind anomaly develops at mid-levels south of ≈ 15° N, representing a weakening of the AEJ's southern flank relative to the modern situation, while the jet slightly intensifies at its northern flank (Fig. 4a–d), implying a northward shift of the jet. This behaviour is more pronounced in the OAV simulations than in their non-DGVM counterparts OAV_f (Fig. 4e and f).

A close relationship exists between surface-temperature anomalies and mid-level wind anomalies over West Africa (Fig. 4). According to the thermal wind relation, anomalous horizontal temperature gradients induce vertical shear such that negative low-level temperature anomalies (communicated into the lower troposphere from the surface) are on the left of the anomalous mid-level wind vectors (cf. Cook, 1999). The negative surface temperature anomalies in the early and mid-Holocene experiments are substantial (more than 6K in the OAV experiments despite larger incoming short-wave radiation at the top of the atmosphere), in line with temperature reconstructions from groundwater samples (Beyerle et al., 2003), and associated with increased cloudiness due to enhanced convection, reflecting solar radiation back to space (cf. Patricola and Cook, 2007). Even more relevant in the context of vegetation-rainfall feedbacks is enhanced latent surface cooling by larger evapotranspiration in the wetter regions. Table 3 summarizes the changes in the different components of surface evapotranspiration over the Sahara/Sahel region for the set of experiments. With enhanced rainfall in

CPD
10, 2055–2086, 2014

the early and mid-Holocene experiments, evapotranspiration increases. This increase is much stronger when dynamic vegetation is enabled (OAV) due to enhanced canopy evaporation and transpiration in the "greener" regions. In the early and mid-Holocene experiments with fixed vegetation (OAV_f and OA) changes in canopy evaporation and transpiration are negligible, whereas ground evaporation substantially increases. This increase in ground evaporation, however, is much smaller than the rise in canopy evaporation and transpiration in the OAV experiments. As a result, latent surface cooling and hence changes in the AEJ are much more pronounced in the early and mid-Holocene experiments with dynamic vegetation (Fig. 4e and f).

Previous work has shown that the AEJ plays a key role in controlling sub-Saharan precipitation by transporting moisture off the continent below the level of condensation, thus increasing moisture divergence over West Africa (e.g. Cook, 1999; Rowell, 2003). Figure 5 displays moisture transport anomalies at the AEJ level for the early and mid-Holocene experiments. In all experiments, eastward moisture flux anomalies appear at the southern flank of the AEJ south of 15° N, effectively reducing the westward moisture export from the North African region to the Atlantic. Owing to a stronger mid-level circulation change, the moisture export across the West African coastline is more strongly reduced in the early and mid-Holocene experiments with interactive dynamic vegetation compared to their fixed-vegetation counterparts (Fig. 5e and f), thus keeping more moisture available to feed the rain in the West African monsoon region.

Initializing the 0k and 6k simulations of CCSM3-DGVM with the expanded North African vegetation cover from experiment 9k(OAV) (cf. Fig. 2b) rather than with bare soil has a negligible effect on the region-averaged (10° N–25° N, 20° W–30° E) precipitation and evapotranspiration (see experiments 0k9k(OAV) and 6k9k(OAV) in Tables 2 and 3). A closer inspection of the North African precipitation fields, however, reveals small but statistically significant differences between the experiments 0k9k(OAV) and 0k(OAV) in a region between 10° N and 15° N (Fig. 6a and c). No such coherent pattern is found for the precipitation difference between experiments 6k9k(OAV) and 6k(OAV), suggesting

CPD
10, 2055–2086, 2014

that there is no significant influence of the initial vegetation cover on CCSM3-DGVM's simulation of mid-Holocene climate in North Africa (Fig. 6b and c).

4 Discussion

In response to enhanced summer insolation CCSM3-DGVM simulates increased rainfall over North Africa along with a northward shift of the monsoon trough during the early and middle Holocene. In the model experiments, higher rainfall is simulated at 9 ka than at 6 ka BP due to stronger insolation forcing. This result should be taken with care, however, since other forcings than orbital and greenhouse gases were not taken into account. In particular, remnants of the Laurentide ice sheet and enhanced meltwater flux into the adjacent ocean might have affected North African rainfall during the early Holocene (Niedermeyer et al., 2009; Lézine et al., 2011; Marzin et al., 2013). Early-to-mid Holocene wet conditions are also simulated for southern Arabia in accordance with geological evidence (e.g. McClure, 1976; Hoelzmann et al., 1998; Fleitmann et al., 2003).

The early and mid-Holocene North African precipitation increase goes along with a northward expansion of the vegetation cover. Substantial greening is also simulated over the Arabian Peninsula in line with vegetation reconstructions (e.g. Hoelzmann et al., 1998). Our sensitivity experiments reveal that the expansion of vegetation acts as a positive feedback on the rainfall increase in both North Africa and the Arabian Peninsula. In the Sahara/Sahel region (10° N–25° N, 20° W–30° E) the dynamic vegetation enhances the orbitally triggered rainfall anomaly by approximately 20 % in both the early and mid-Holocene experiments. Despite the enhanced anomalous rainfall when dynamic vegetation is enabled, CCSM3-DGVM still underestimates early-to-mid Holocene monsoonal rainfall in the Saharan region by roughly a factor of two when compared to mid-Holocene reconstructions (Bartlein et al., 2011). Likewise, the northward expansion of savanna-type vegetation in North Africa also seems to be undersimulated (e.g. Hoelzmann et al., 1998; Jolly et al., 1998; Prentice et al.,

CPD
10, 2055–2086, 2014

2000). Underestimation of the northward extent and intensity of precipitation (and vegetation) changes is a common problem in coupled climate model simulations of the mid-Holocene (e.g. Zheng and Braconnot, 2013), which might reflect shortcomings in physical model parameterizations and/or missing land surface feedbacks (soil, lakes) or could be related to coarse model resolution (Bosmans et al., 2012).

A closer inspection of the mid-tropospheric wind field has identified changes in the AEJ as a key component of the positive vegetation-precipitation feedback mechanism in CCSM3-DGVM. More vegetation north of 15° N facilitates enhanced latent surface cooling through canopy evaporation and transpiration which, according to the thermal wind balance, results in a substantial deceleration of the jet's southern flank associated with a northward AEJ shift. Previous work has shown that a slowdown and/or northward shift of the AEJ is associated with positive Sahelian rainfall anomalies (e.g. Rowell et al., 1992; Xue and Shukla, 1993, 1996; Cook, 1999; Nicholson and Grist, 2001; Rowell, 2003; Cook and Vizy, 2006; Patricola and Cook, 2007; Nicholson, 2008; Bouimetarhan et al., 2012). A latitudinal displacement of the AEJ may affect Sahel rainfall through changes in horizontal and vertical wind shear and associated dynamic instabilities (Grist and Nicholson, 2001; Nicholson and Grist, 2001), a mechanism poorly resolved in coarse-resolution global climate models. Another way to connect changes in the AEJ with rainfall anomalies is through the large-scale column moisture budget (Cook, 1999; Rowell, 2003; Patricola and Cook, 2007; Mulitza et al., 2008). The mid-level jet plays a major role in the North African moisture budget by exporting large amounts of water vapor from the continent to the Atlantic Ocean below the level of condensation. Calculation of horizontal vapour transports in our experiments has revealed a reduction of this moisture export out of the North African realm in the early and middle Holocene. This reduction is amplified by stronger surface cooling in the OAV experiments with dynamic vegetation (Fig. 4e and f), such that more moisture is available to feed the rain in the monsoonal region, providing for a positive vegetation-precipitation feedback.

A positive feedback between the AEJ and sub-Saharan rainfall has been suggested in previous studies (Rowell et al., 1992; Cook, 1999; Rowell, 2003). Our experiments

CPD
10, 2055–2086, 2014

suggest that this feedback is boosted by a dynamic vegetation cover through modification of surface latent heat fluxes and low-level temperature gradients. As such, our results are largely consistent with the regional atmosphere model simulations by Patricola and Cook (2008) who found a close link between Saharan/Sahelian vegetation, North African rainfall, and moisture transports by the AEJ, whereas changes in vegetation have almost no effect on the southerly surface winds from the Gulf of Guinea and the associated low-level moisture import to the West African monsoon system. However, contrary to Patricola and Cook (2008) who found increasing low-level moist static energy and hence increasing convective instability where vegetation expands, changing vegetation has no effect on low-level moist static energy in our CCSM3-DGVM simulations (not shown).

The positive vegetation-precipitation feedback via mid-tropospheric atmosphere dynamics (AEJ) identified in our model experiments is induced by changes in surface latent heat fluxes. Water vapor, and hence latent heat, is introduced into the atmosphere via plant transpiration and the evaporation of water from the soil and free water on the vegetation canopy (the summed rate is called evapotranspiration). An expanded vegetation cover in North Africa during the early-to-mid Holocene favours evapotranspiration (cf. Ripley, 1976). Evapotranspiration increases with precipitation, but the slope is steeper when dynamic vegetation is enabled (Fig. 7). Whether the additional moisture introduced into the atmosphere from the expanded vegetation canopy contributes to enhanced rainfall through local water recycling has been assessed by calculating the Budyko recycling coefficient (representing the ratio of total precipitation to advected precipitation over a specified area) as defined by Brubaker et al. (1993) for the Sahara/Sahel region (10° N–25° N, 20° W–30° E). We found that enhanced water recycling plays no role in the model's positive vegetation-rainfall feedback. For instance, the regional recycling coefficient surprisingly decreases from 1.98 in the pre-industrial control run 0k(OAV) to 1.59 in the early Holocene experiment 9k(OAV) when dynamic vegetation is enabled, whereas it increases from 1.66 (pre-industrial) to 2.03 (early Holocene) in the fixed-vegetation experiments 0k(OAV_f) and 9k(OAV_f), respectively.

CPD
10, 2055–2086, 2014

A closer inspection of the changes in evapotranspiration reveals enhanced evaporative surface cooling due to canopy evaporation and transpiration during the early-to-mid Holocene. Model studies who have shown a negative vegetation-precipitation feedback in North Africa (Liu et al., 2007, 2010) did not include a canopy evaporation term in the formulation of surface hydrology. However, including canopy evaporation in our simulations is crucial for obtaining enough evaporative surface cooling to trigger the positive vegetation-precipitation feedback via mid-tropospheric atmosphere dynamics. In fact, if canopy evaporation was neglected in our simulations (and would not have been compensated by enhanced transpiration or ground evaporation), the feedback would disappear or even become negative (cf. Table 3).

Vegetation-induced changes in surface albedo (Charney feedback), which would increase low-level moist static energy (resulting in atmospheric destabilization) through enhanced surface warming – or more precisely, less pronounced surface cooling (Charney, 1976) – play no substantial role for creating a positive vegetation-rainfall feedback in our model study, unlike in earlier studies (e.g. Kutzbach et al., 1996; Claussen and Gayler, 1997; Hales et al., 2006). By contrast, the positive feedback through AEJ dynamics as found in our study relies on North African surface cooling rather than enhanced surface warming by decreasing surface albedo, consistent with the regional model study by Patricola and Cook (2008). It is important to note that soil albedoes in CCSM3-DGVM depend on the volumetric water content of the first soil layer and can locally be as small as 0.09 for saturated soils in the visible range (Oleson et al., 2004). This strongly diminishes the effect of vegetation on North African surface albedo (Levis et al., 2004a; Notaro et al., 2008).

The results from experiments 0k9k(OAV) and 6k9k(OAV) suggest that the simulation of modern and mid-Holocene regional climate in North Africa does not depend on the initial vegetation cover. Despite the existence of a positive vegetation-rainfall feedback multiple equilibrium states were not found on the regional scale, which would rule out the potential for abrupt climate-vegetation transitions in the Holocene due to a catastrophic bifurcation or "unstable collapse" (Liu et al., 2006, 2007). However, statistical

CPD
10, 2055–2086, 2014

significance tests did not rule out the possibility of multiple states at the local scale between 10° N and 15° N under modern boundary conditions. This implies that, locally, unstable collapses could occur such that late Holocene proxy records from specific sites may show abrupt transitions while records from other sites do not (cf. Bathiany et al., 2012). Similar ideas were put forward by Williams et al. (2011) and Brovkin and Claussen (2008). For the middle Holocene, the climate-ecosystem turned out to be mono-stable in CCSM3-DGVM even at the local scale, which is consistent with earlier findings by Brovkin et al. (1998) who suggested that the system is prone to bi-stability only in the late Holocene, whereas the early-to-mid Holocene was mono-stable.

5 Conclusions

Model experiments with CCSM3-DGVM support the findings of increased summer rainfall and expansion of vegetation in the early-to-mid Holocene over North Africa as in previous coupled general circulation model studies. By enabling interactive dynamic vegetation (OAV experiments), rainfall intensification is much more pronounced in this model. In the Sahara/Sahel region, the dynamic vegetation enhances the orbitally triggered summer rainfall anomaly by approximately 20 % in both the early (9 ka BP) and mid-Holocene (6 ka BP) experiments. The primary vegetation-atmosphere feedback identified here operates through surface latent heat flux anomalies by canopy evapotranspiration and their effect on the AEJ. As such, the vegetation feedback relies on enhanced surface (evaporational) cooling as opposed to the Charney feedback which operates through atmospheric instability by decreased surface albedo. Neglecting canopy evaporation, as in some previous model studies, could substantially affect the simulation of evaporative cooling such that the positive vegetation-atmosphere feedback might disappear. Even though CCSM3-DGVM simulates a positive vegetation-precipitation feedback over North Africa, this feedback is not strong enough to produce multiple equilibrium climate-ecosystem states on a regional scale.

CPD
10, 2055–2086, 2014

Acknowledgements. This study has been supported by the Deutsche Forschungsgemeinschaft (DFG) through the Priority Programme INTERDYNAMIC. The CCSM3-DGVM model simulations have been carried out on the HLRN-II (SGI Altix) supercomputer.

References

Bartlein, P. J., Harrison, S. P., Brewer, S., Connor, S., Davis, B. A. S., Gajewski, K., Guiot, J., Harrison-Prentice, T. I., Henderson, A., Peyron, O., Prentice, I. C., Scholze, M., Seppa, H., Shuman, B., Sugita, S., Thompson, R. S., Viau, A. E., Williams, J., Wu, H.: Pollen-based continental climate reconstructions at 6 and 21 ka: A global synthesis, Clim. Dynam, 37, 775–802, 2011. 2056, 2064

Bathiany, S., Claussen, M., and Fraedrich, K.: Implications of climate variability for the detection of multiple equilibria and for rapid transitions in the atmosphere-vegetation system, Clim. Dynam., 38, 1775–1790, 2012. 2057, 2068

Berger, A.: Long-term variations of daily insolation and Quaternary Climatic Changes, J. Atmos. Sci., 35, 2362–2367, 1978. 2060

Beyerle, U., Rueedi, J., Leuenberger, M., Aeschbach-Hertig, W., Peeters, F., Kipfer, R., and Dodo, A.: Evidence for periods of wetter and cooler climate in the Sahel between 6 and 40 kyr BP derived from groundwater, Geophys. Res. Lett., 30, 1173, doi:10.1029/2002GL016310, 2003. 2062

Bonan, G. B. and Levis, S.: Evaluating aspects of the Community Land and Atmosphere Models (CLM3 and CAM) using a dynamic global vegetation model, J. Climate, 19, 2290–2301, 2006. 2059

Bonan, G. B., Levis, S., Sitch, S., Vertenstein, M., and Oleson, K. W.: A dynamic global vegetation model for use with climate models: concepts and description of simulated vegetation dynamics, Global Change Biol., 9, 1543–1566, 2003. 2061

Bosmans, J. H. C., Drijfhout, S. S., Tuenter, E., Lourens, L. J., Hilgen, F. J., and Weber, S. L.: Monsoonal response to mid-holocene orbital forcing in a high resolution GCM, Clim. Past, 8, 723–740, doi:10.5194/cp-8-723-2012, 2012. 2065

Bouimetarhan, I., Prange, M., Schefuss, E., Dupont, L., Lippold, J., Mulitza, S., and Zonneveld, K.: Sahel megadrought during Heinrich Stadial 1: evidence for a three-phase evolution of the low- and mid-level West African wind system, Quaternary Sci. Rev., 58, 66–76, 2012. 2065

CPD
10, 2055–2086, 2014

Braconnot, P., Otto-Bliesner, B., Harrison, S., Joussaume, S., Peterchmitt, J.-Y., Abe-Ouchi, A., Crucifix, M., Driesschaert, E., Fichefet, Th., Hewitt, C. D., Kageyama, M., Kitoh, A., Laîné, A., Loutre, M.-F., Marti, O., Merkel, U., Ramstein, G., Valdes, P., Weber, S. L., Yu, Y., and Zhao, Y.: Results of PMIP2 coupled simulations of the Mid-Holocene and Last Glacial Maximum – Part 1: experiments and large-scale features, Clim. Past, 3, 261–277, doi:10.5194/cp-3-261-2007, 2007. 2058, 2059, 2061

Brovkin, V. and Claussen, M.: Comment on Climate-Driven Ecosystem Succession in the Sahara: The Past 6000 Years, Science, 322, 1326, doi:10.1126/science.1163381, 2008. 2068

Brovkin, V., Claussen, M., Petoukhov, V., and Ganopolski, A.: On the stability of the atmosphere-vegetation system in the Sahel/Sahara region, J. Geophys. Res., 103, 31613–31624, 1998. 2057, 2068

Brubaker, K. L., Entekhabi, D., and Eagleson, P. S.: Estimation of continental precipitation recycling, J. Climate, 6, 1077–1089, 1993. 2066

Charney, J. G.: Dynamics of deserts and drought in the Sahel, Q. J. Roy. Meteorol. Soc., 101, 193–202, 1975. 2057

Charney, J. G., Stone, P. H., and Quirk, W. J.: Reply, Science, 191, 100–102, 1976. 2067

Claussen, M.: On coupling global biome models with climate models, Climate Res., 4, 203–221, 1994. 2057

Claussen, M.: Modelling biogeophysical feedback in the African and Indian Monsoon region, Clim. Dynam., 13, 247–257, 1997. 2057

Claussen, M.: On multiple solutions of the atmosphere-vegetation system in present-day climate, Global Change Biol., 5, 549–559, 1998. 2057

Claussen, M.: Late Quaternary vegetation-climate feedbacks, Clim. Past, 5, 203–216, doi:10.5194/cp-5-203-2009, 2009. 2057

Claussen, M. and Gayler, V.: The greening of Sahara during the mid-Holocene: Results of an interactive atmosphere-biome model, Global Ecol. Biogeogr., 6, 369–377, 1997. 2057, 2067

Claussen, M., Brovkin, V., Ganopolski, A., Kubatzki, C., and Petoukhov, V.: Modeling global terrestrial vegetation-climate interaction, Philos. T. Roy. Soc. Lond. B, 353, 53–56, doi:10.1098/rstb.1998.0190, 1998. 2057

Claussen, M., Kubatzki, C., Brovkin, V., Ganopolski, A., Hoelzmann, P., Pachur, H. J.: Simulation of an abrupt change in Saharan vegetation in the mid-Holocene, Geophys. Res. Lett., 26, 2037–2040, doi:10.1029/1999GL900494, 1999. 2057

CPD
10, 2055–2086, 2014

Coe, M. and Bonan, G.: Feedbacks between climate and surface water in northern Africa during the middle Holocene, J. Geophys. Res., 102, 11087–11101, doi:10.1029/97JD00343, 1997. 2057

Collins, W. D., Bitz, C. M., Blackmon, M. L., Bonan, G. B., Bretherton, C. S., Carton, J. A., Chang, P., Doney, S. C., Hack, J. J., Henderson, T. B., Kiehl, J. T., Large, W. G., McKenna, D. S., Santer, B. D., and Smith, R. D.: The Community Climate System Model version 3 (CCSM3), J. Climate, 19, 2122–2143, 2006. 2059

Collins, J. A., Schefuss, E., Mulitza, S., Prange, M., Werner, M., Tharammal, T., Paul, A., and Wefer, G.: Estimating the hydrogen isotopic composition of past precipitation using leaf-waxes from western Africa, Quaternary Sci. Rev., 65, 88–101, 2013. 2056

Cook, K. H.: Generation of the African Easterly Jet and Its Role in Determining West African Precipitation, J. Climate, 12, 1165–1184, 1999. 2062, 2063, 2065

Cook, K. H., and Vizy, E. K.: Coupled model simulations of the West African monsoon system: Twentieth- and twenty-first-century simulations, J. Climate, 19, 3681–3703, 2006. 2065

DeFries, R. S., Townshend, J. R. G., and Hansen, M. C.: Continuous fields of vegetation characteristics at the global scale at 1 km resolution, J. Geophys. Res., 104, 16911–16925, 1999. 2061

DeFries, R. S., Hansen, M. C., Townshend, J. R. G., Janetos, A. C., Loveland, T. R.: A new global 1-km dataset of percentage tree cover derived from remote sensing, Global Change Biol., 6, 247–254, 2000. 2061

deMenocal, P., Ortiz, J., Guilderson, T., Adkins, J., Sarnthein, M., Baker, L., and Yarusinsky, M.: Abrupt onset and termination of the African humid period: Rapid climate responses to gradual insolation forcing, Quaternary Sci. Rev., 19, 347–361, 2000. 2057

Doherty, R. M., Kutzbach, J., Foley, J., and Pollard, D.: Fully- coupled climate/dynamical vegetation model simulations over Northern Africa during the mid-Holocene, Clim. Dynam., 16, 561–567, 2000. 2057

Fleitmann, D., Burns, S. J., Mudelsee, M., Neff, U., Kramers, J., Mangini, A., and Matter, A.: Holocene forcing of the Indian monsoon recorded in a stalagmite from Southern Oman, Science, 300, 1737–1739, 2003. 2064

Francus, P., von Suchodoletz, H., Dietze, M., Donner, R. V., Bouchard, F., Roy, A.-J., Fagot, D., Verschuren, D., and Kröpelin, S.: Varved sediments of Lake Yoa (Ounianga Kebir, Chad) reveal progressive drying of the Sahara during the last 6100 years, Sedimentology, 60, 911–934, doi:10.1111/j.1365-3091.2012.01370.x, 2013. 2058

CPD
10, 2055–2086, 2014

Grist, J. P. and Nicholson, S. E.: A study of the dynamic factors influencing the interannual variability of rainfall in the West African Sahel, J. Climate, 14, 1337-1359, 2001. 2065

Hales, K., Neelin, J. D., and Zeng, N.: Interaction of vegetation and atmospheric dynamical mechanisms in the mid-holocene African monsoon, J. Climate, 19, 4105–4120, 2006. 2057, 2067

Handiani, D., Paul, A., Prange, M., Merkel, U., Dupont, L., and Zhang, X.: Tropical vegetation response to Heinrich Event 1 as simulated with the UVic ESCM and CCSM3, Clim. Past, 9, 1683–1696, doi:10.5194/cp-9-1683-2013, 2013. 2059

Hoelzmann, P., Jolly, D., Harrison, S. P., Laarif, F., Bonnefille, R., and Pachur, H. J.: Mid-Holocene land surface conditions in northern Africa and the Arabian Peninsula: A data set for the analysis of biogeochemical feedbacks in the climate system, Global Biogeochem. Cy., 12, 35–52, 1998. 2064

Jolly, D., Harrison, S. P., Damnati, B., and Bonnefille, R.: Simulated climate and biomes of Africa during the Late Quaternary: comparison with pollen and lake status data, Quaternary Sci. Rev., 17, 629–657, 1998. 2056, 2057, 2064

Kohfeld, K. E. and Harrison, S. P.: How well can we simulate past climates? Evaluating the models using global palaeoenvironmental datasets, Quaternary Sci. Rev., 19, 321–345, 2000. 2056, 2057

Krinner, G., Lézine, A.-M., Braconnot, P., Sepulchre, P., Ramstein, G., Grenier, C., and Gouttevin, I.: A reassessment of lake and wetland feedbacks on the North African Holocene climate, Geophys. Res. Lett., 39, L07701, doi:10.1029/2012GL050992, 2012. 2057

Kröpelin, S., Verschuren, D., Lézine, A.-M., Eggermont, H., Cocquyt, C., Francus, P., Cazet, J.-P., Fagot, M., Rumes, B., Russell, J. M., Darius, F., Conley, D. J., Schuster, M., von Suchodoletz, H., and Engstrom, D. R.: Climate-driven ecosystem succession in the Sahara: The past 6000 years, Science, 320, 765–768, 2008. 2058

Kutzbach, J. E.: Monsoon Climate of the Early Holocene- Climate Experiment with the Earths Orbital Parameters for 9000 years ago, Science, 214, 59–61, 1981. 2056

Kutzbach, J. E. and Liu, Z.: Response of the African monsoon to orbital forcing and ocean feedbacks in the middle Holocene, Science, 278, 440–444, 1997. 2057

Kutzbach, J. E. and Street-Perrot, E. A.: Milankovitch Forcing of Fluctuations in the Level of Tropical Lakes from 18 to 0 ka, Nature, 317, 130–134, 1985. 2056

CPD
10, 2055–2086, 2014

Kutzbach, J. E., Bonan, G., Foley, J., and Harrison, S. P.: Vegetation/soil feedbacks and African monsoon response to orbital forcing in the Holocene, Nature, 384, 623–626, 1996. 2057, 2067

Lawrence, P. J., and Chase, T. N.: Representing a new MODIS consistent land surface in the Community Land Model (CLM3.0), J. Geophys. Res., 112, G01023, doi:10.1029/2006JG000168, 2007. 2061

Levis, S., Bonan, G. B., and Bonfils, C.: Soil feedback drives the Mid-Holocene North African monsoon northward in fully coupled CCSM2 simulations with a dynamic vegetation model, Clim. Dynam., 23, 791–802, 2004a. 2057, 2058, 2067

Levis, S., Bonan, G. B., Vertenstein, M., and Oleson, K. W.: The Community Land Model's Dynamic Global Vegetation Model (CLM-DGVM): Technical description and user's guide, NCAR Technical Note NCAR/TN-459+IA, National Center for Atmospheric Research, Boulder, CO, 2004b. 2059

Lézine, A., Hély, C., Grenier, C., Braconnot, P., Krinner, G.: Sahara and Sahel vulnerability to climate changes, lessons from Holocene hydrological data, Quaternary Sci. Rev., 30, 3001–3012, 2011. 2058, 2064

Liu, Z., Wang, Y., Gallimore, R., Notaro, M., and Prentice, C. I.: On the mechanism of abrupt change of Northern Africa environment in the Holocene: climate variability vs. vegetation feedback, Geophys. Res. Lett., 33, L22709, doi:10.1029/2006GL028062, 2006. 2057, 2058, 2067

Liu, Z., Wang, Y., Gallimore, R., Gasse, F., Johnson, T., deMenocal, P., Adkins, J., Notaroa, M., Prentice, I. C., Kutzbach, J., Jacob, R., Behling, P., Wang, L., and Ong, E.: Simulating the transient evolution and abrupt change of Northern Africa atmosphere-ocean-terrestrial ecosystem in the Holocene, Quaternary Sci. Rev., 26, 1818–1837, 2007. 2057, 2058, 2067

Liu, Z., Notaro, M., and Gallimore, R.: Indirect vegetation soil moisture feedback with application to Holocene North Africa climate, Global Change Biol., 16, 1733–1743, 2010. 2058, 2067

Marzin, C., Braconnot, P., Kageyama, M.: Relative impacts of insolation changes, meltwater fluxes and ice sheets on African and Asian monsoons during the Holocene, Clim Dyn 41:2267-2286, 2013. 2064

McClure, H. A.: Radiocarbon chronology of late Quaternary lakes in the Arabian Desert, Nature, 263, 755–756, 1976. 2064

CPD
10, 2055–2086, 2014

Mulitza, S., Prange, M., Stuut, J. B., Zabel, M., von Dobeneck, T., Itambi, C. A., Nizou, J., Schulz, M., and Wefer, G.: Sahel megadroughts triggered by glacial slowdowns of Atlantic meridional overturning, Paleoceanography 23, PA4206, doi:10.1029/2008PA001637, 2008. 2065

Nicholson, S. E.: The intensity, location and structure of the tropical rainbelt over West Africa as a factor in interannual variability, Int. J. Climatol., 28, 1775–1785, 2008. 2065

Nicholson, S. E. and Grist, J. P.: A conceptual model for understanding rainfall variability in the West African Sahel on interannual and interdecadal timescales, Int. J. Climatol., 21, 1733–1757, 2001. 2065

Niedermeyer, E. M., Prange, M., Mulitza, S., Mollenhauer, G., Schefuss, E., and Schulz, M.: Extratropical forcing of Sahel aridity during Heinrich stadials, Geophys. Res. Lett. 36, L20707, doi:10.1029/2009GL039687, 2009. 2064

Notaro, M., Wang, Y., Liu, Z., Gallimore, R., and Levis, S.: Combined statistical and dynamical assessment of simulated vegetation-rainfall interactions in North Africa during the mid-Holocene, Global Change Biol., 14, 347–368, 2008. 2058, 2067

Oleson, K. W., Dai, Y., Bonan, G., Dickinson, R. E., Dirmeyer, P. A., Hoffman, F., Houser, P., Levis, S., Niu, G.-Y., Thornton, P., Vertenstein, M., Yang, Z.-L., and Zeng, X.: Technical description of the Community Land Model (CLM), Tech. Rep. NCAR/TN-461, National Center for Atmospheric Research, Boulder, CO, 174 pp., 2004. 2067

Oleson, K. W., Niu, G. Y., Yang, Z. L., Lawrence, D. M., Thornton, P. E., Lawrence, P. J., Stockli, R., Dickinson, R. E. G., Bonan, B., Levis, S., Dai, A., and Qian, T.: Improvements to the Community Land Model and their impact on the hydrological cycle, J. Geophys. Res., 113, G01021, doi:10.1029/2007JG000563, 2008. 2059, 2061

Otterman, J.: Baring high-albedo soils by overgrazing: a hypothesised desertification mechanism, Science, 186, 531–533, 1974. 2057

Otto-Bliesner, B. L., Tomas, R., Brady, E. C., Ammann, C., Kothavala, Z., and Clauzet, G.: Climate sensitivity of moderate and low–resolution versions of CCSM3 to preindustrial forcings, J. Climate, 19, 2567–2583, 2006. 2060

Patricola, C. M. and Cook, K. H.: Dynamics of the West African Monsoon under Mid-Holocene Precessional Forcing: Regional Climate Model Simulations, J. Climate, 20, 694–716, 2007. 2062, 2065

CPD
10, 2055–2086, 2014

Patricola, C. M. and Cook, K. H.: Atmosphere/vegetation feedbacks: A mechanism for abrupt climate change over northern Africa, J. Geophys. Res., 113, D18102, doi:10.1029/2007JD009608, 2008. 2057, 2058, 2066, 2067

Prentice, I. C. and Jolly, D.: BIOME 6000 participants: Mid-Holocene and glacial-maximum vegetation geography of the northern continents and Africa, J. Biogeogr., 27, 507–519, 2000. 2056, 2064

Renssen, H., Brovkin, V., Fichefet, T., and Goosse, H.: Holocene climate instability during the termination of the African Humid Period, Geophys. Res. Lett., 30, 1184, doi:10.1029/2002GL016636, 2003. 2057

Ripley, E. A.: Drought in the Sahara: insufficient bio-geophysical feedback?, Science, 191, 100–102, doi:10.1126/science.191.4222.100, 1976. 2066

Rowell, D. P.: The impact of Mediterranean SSTs on the Sahelian rainfall Season, J. Climate, 16, 849–862, 2003. 2063, 2065

Rowell, D. P., Folland, C. K., Maskell, K., Owen, J. A., and Ward, M. N.: Modelling the influence of global sea surface temperatures on the variability and predictability of seasonal Sahel rainfall, Geophys. Res. Lett., 19, 905–908, 1992. 2065

Sitch, S., Smith, B., Prentice, I. C., Arneth, A., Bondeau, A., Cramer, W., Kaplan, J. O., Levis, S., Lucht, W., Sykes, M. T., Thonicke, K., and Venevsky, S.: Evaluation of ecosystem dynamics, plant geography and terrestrial carbon cycling in the LPJ dynamic vegetation model, Global Change Biol., 9, 161–185, 2003. 2059, 2061

Street-Perrott, F. A. and Perrott, R. A.: Holocene vegetation, lake levels and climate of Africa, in: Global climates since the Last Glacial Maximum, University of Minnesota Press, Minneapolis, 318–356, 1993. 2056

Wang, G. and Eltahir, E. A. B.: Biosphere-Atmosphere Interactions over West Africa, 2. Multiple Equilibria, Q. J. Roy. Meteorol. Soc., 126, 1261–1280, 2000. 2057

Wang, Y., Notaro, M., Liu, Z., Gallimore, R., Levis, S., and Kutzbach, J. E.: Detecting vegetation-precipitation feedbacks in mid-Holocene North Africa from two climate models, Clim. Past, 4, 59–67, doi:10.5194/cp-4-59-2008, 2008. 2058

Williams, J. W., Blois, J. L., and Shuman, B. N.: Extrinsic and intrinsic forcing of abrupt ecological change: case studies from the late Quaternary, J. Ecol., 99, 664–677, 2011. 2068

Xue, Y. and Shukla, J.: The influence of land-surface properties on Sahel climate, Part 1: Desertification, J. Climate, 6, 2232–2245, 1993. 2065

CPD
10, 2055–2086, 2014

Xue, Y. and Shukla, J.: The influence of land surface properties on Sahel climate, Part II: Afforestation, J. Climate, 9, 3260–3275, 1996. 2065

Yeager, S. G., Shields, C. A., Large, W. G., and Hack, J. J.: The low-resolution CCSM3, J. Climate, 19, 2545–2566, 2006. 2059

Zeng, N. and Neelin, J. D.: The Role of Vegetation-Climate Interaction and Interannual Variability in Shaping the African Savanna, J. Climate, 13, 2665–2670, 2000. 2057

Zhao, Y. and Harrison, S. P.: Mid-Holocene monsoons: A multi-model analysis of the interhemispheric differences in the responses to orbital forcing and ocean feedbacks, Clim. Dynam., 39, 1457–1487, 2012. 2057

Zhao, Y., Braconnot, P., Marti, O., Harrison, S. P., Hewitt, C., Kitoh, A., Liu, Z., Mikolajewicz, U., Otto-Bliesner, B., and Weber, S. L.: A Multi-Model Analysis of the Role of the Ocean on the African and Indian Monsoon During the Mid-Holocene, Clim. Dynam., 25, 777–800, 2005. 2057

Zheng, W. and Braconnot, P.: Characterization of Model Spread in PMIP2 Mid-Holocene Simulations of the African Monsoon, J. Climate, 26, 1192–1210, 2013. 2065

CPD
10, 2055–2086, 2014

Table 1. Summary of boundary conditions used in the experiments. Summer insolation refers to 21 July at 20° N.

Experiments	CO_2 (ppmv)	CH_4 (ppbv)	N_2O (ppbv)	Summer insolation ($W\,m^{-2}$)
0k (PI)	280	760	270	453
6k (mid-Holocene)	280	650	270	477
9k (early Holocene)	265	680	260	486

CPD
10, 2055–2086, 2014

Table 2. Mean summer (JJAS) precipitation over the region 10° N–25° N, 20° W–30° E in the various experiments. ΔP denotes anomalies relative to the corresponding 0k (PI) case. SE is the standard error. Precipitation values are normally distributed according to a Shapiro–Wilk normality test (95 % confidence level).

Experiments	Precipitation (P) ± 2 SE (mm day $^{-1}$)	ΔP (mm day $^{-1}$)
0k(OAV)	2.44 ± 0.04	
6k(OAV)	3.41 ± 0.04	0.97
9k(OAV)	3.71 ± 0.04	1.27
0k(OAV_f)	2.47 ± 0.04	
6k(OAV_f)	3.27 ± 0.06	0.80
9k(OAV_f)	3.51 ± 0.06	1.04
0k(OA)	2.48 ± 0.04	
6k(OA)	3.29 ± 0.04	0.81
9k(OA)	3.47 ± 0.06	0.99
0k9k(OAV)	2.47 ± 0.06	< 2 SE
6k9k(OAV)	3.42 ± 0.04	0.98

CPD
10, 2055–2086, 2014

Table 3. Changes of summer canopy evaporation, canopy transpiration and ground evaporation in the various early and mid-Holocene experiments over the region 10° N–25° N, 20° W–30° E.

Experiments	Canopy evaporation (mm day^{-1})	Canopy transpiration (mm day^{-1})	Ground evaporation (mm day^{-1})
6k-0k(OAV)	0.18	0.23	0.06
9k-0k(OAV)	0.23	0.29	0.11
6k-0k(OAV$_f$)	0.00	−0.03	0.34
9k-0k(OAV$_f$)	0.00	−0.03	0.45
6k-0k(OA)	0.00	−0.01	0.29
9k-0k(OA)	0.07	0.04	0.23
0k9k-0k(OAV)	0.03	0.04	−0.04
6k9k-0k(OAV)	0.18	0.22	0.07

CPD
10, 2055–2086, 2014

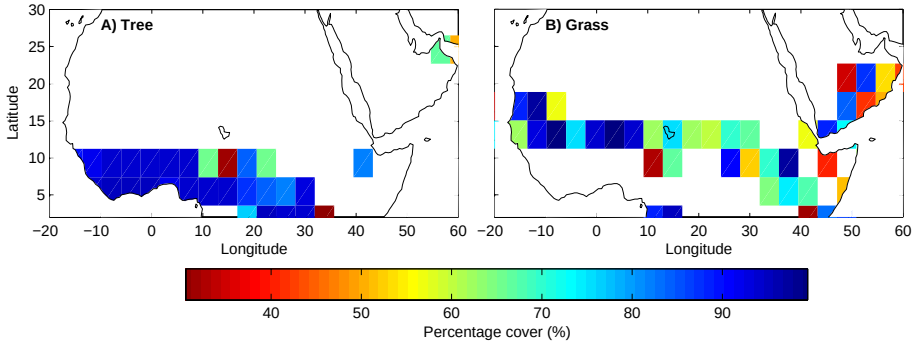

Fig. 1. Pre-industrial vegetation cover over North Africa simulated by CCSM3-DGVM. **(A)** Percentage coverage of tree PFTs, **(B)** same for grasses.

CPD
10, 2055–2086, 2014



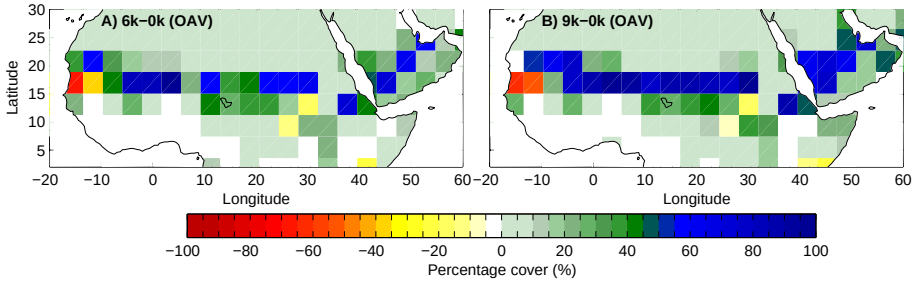

Fig. 2. Change in total (i.e. all PFTs) percent vegetation cover for **(A)** the mid-Holocene (6 ka BP) and **(B)** the early Holocene (9 ka BP) experiment relative to pre-industrial (PI).

CPD
10, 2055–2086, 2014


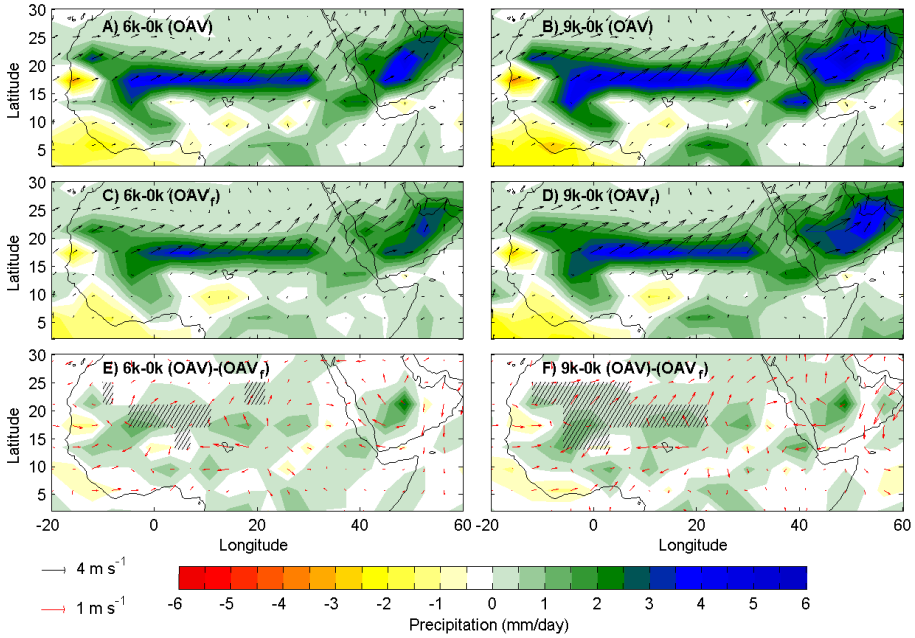

Fig. 3. Changes of summer precipitation and near-surface winds for **(A)** the mid-Holocene and **(B)** the early Holocene experiment relative to PI in model simulations with dynamic vegetation. **(C, D)** Same as **(A, B)** but for fixed-vegetation simulations. **(E, F)** Differences between dynamic vegetation and fixed-vegetation experiments. Hatched areas in **(E, F)** display significant precipitation differences (95 % confidence level) according to both a (non-parametric) Wilcoxon–Mann–Whitney test and a Student *t* test.

CPD
10, 2055–2086, 2014

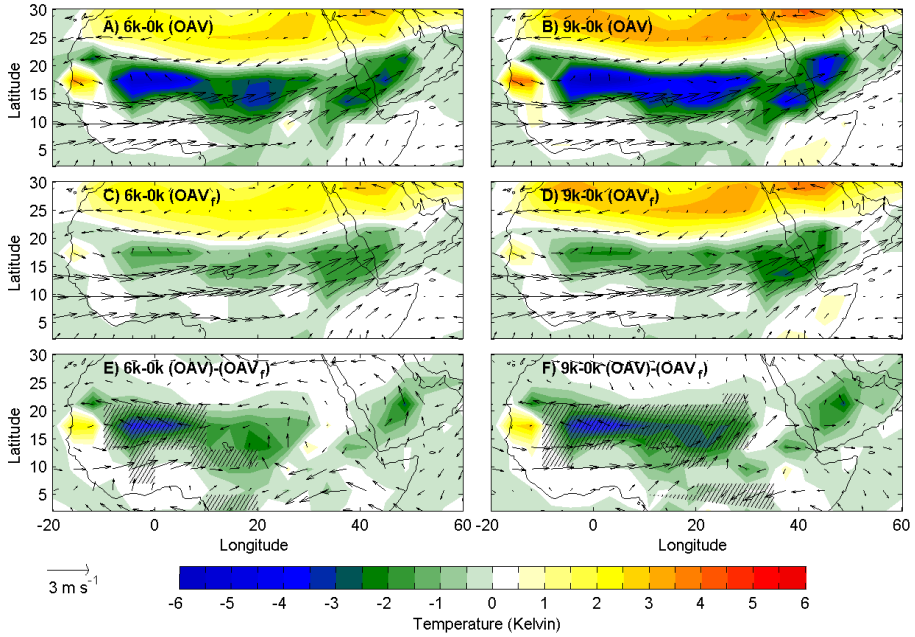

Fig. 4. As in Fig. 3, but for changes in summer surface temperature and 700 hPa winds. Hatched areas in **(E, F)** display significant temperature differences (95 % confidence level) according to both a (non-parametric) Wilcoxon–Mann–Whitney test and a Student *t* test.

CPD
10, 2055–2086, 2014

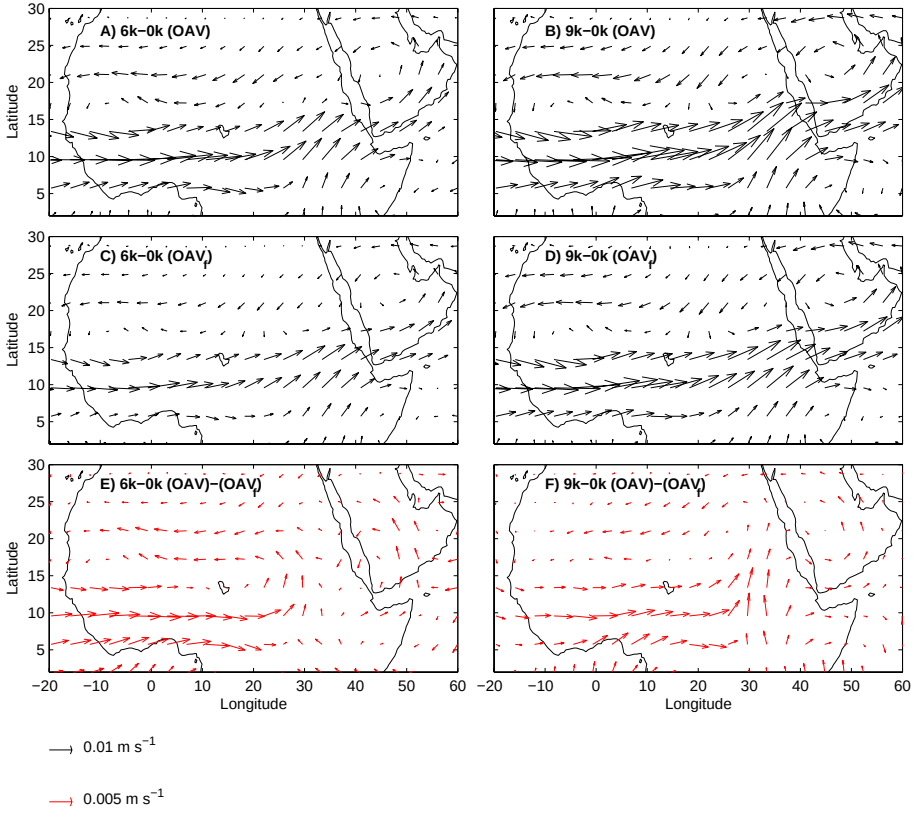

Fig. 5. As in Fig. 3, but for changes in summer moisture transport at 700 hPa.

CPD
10, 2055–2086, 2014

North African vegetation-precipitation feedback

R. Rachmayani et al.

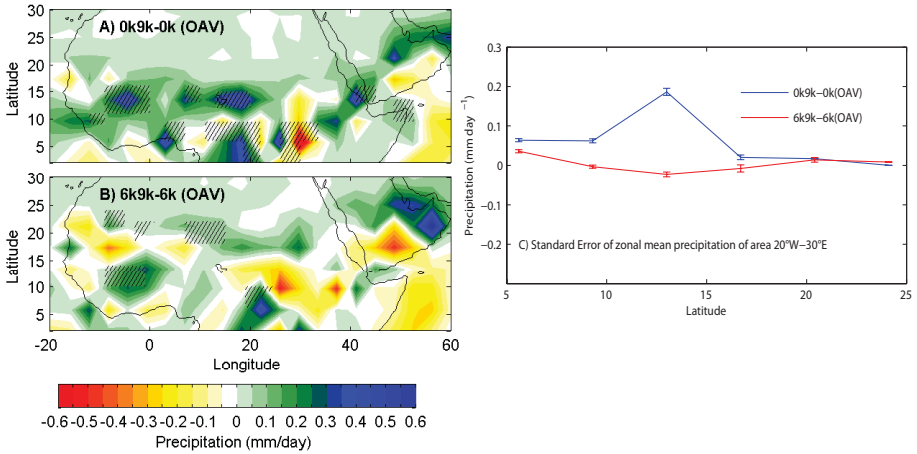

Fig. 6. Influence of vegetation initial conditions (9k North African vegetation cover versus bare soil) on pre-industrial and mid-Holocene North African climate simulations. Shown are differences in summer precipitation for **(A)** 0k9k-0k(OAV) and **(B)** 6k9k-6k(OAV). Hatched areas display significant precipitation differences (95 % confidence level) according to both a (non-parametric) Wilcoxon–Mann–Whitney test and a Student *t* test. **(C)** shows the corresponding zonal averages over North Africa (20° W–30° E) along with standard errors.

CPD
10, 2055–2086, 2014

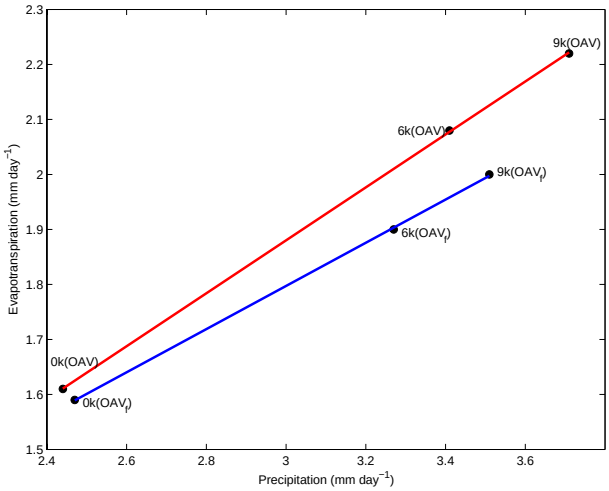

Fig. 7. Mean summer evapotranspiration versus precipitation over the region 10° N–25° N, 20° W–30° E in the 0k, 6k and 9k experiments with dynamic vegetation (OAV experiments; red) and with fixed vegetation (OAV_f experiments; blue).

CPD
10, 2055–2086, 2014